Biophysical Journal, Volume *120*

Supplemental information

EGGTART: A tool to visualize the dynamics of biophysical transport under the inhomogeneous l-TASEP

Dan D. Erdmann-Pham, Wonjun Son, Khanh Dao Duc, and Yun S. Song

Supporting Material

EGGTART: A computational tool to visualize the dynamics of biophysical transport processes under the inhomogeneous ℓ-TASEP

Dan D. Erdmann-Pham[1], Wonjun Son[2], Khanh Dao Duc[3] and Yun S. Song[4,5,6,*]

1 Department of Mathematics, University of California, Berkeley, CA 94720, USA
2 Department of Computer Science, Columbia University, New York, NY 10027, USA
3 Department of Mathematics, University of British Columbia, Vancouver, BC V6T 1Z4, Canada
4 Computer Science Division, University of California, Berkeley, CA 94720, USA
5 Department of Statistics, University of California, Berkeley, CA 94720, USA
6 Chan Zuckerberg Biohub, San Francisco, CA 94158, USA

* Lead Contact and Corresponding Author: yss@berkeley.edu

This Supplemental Information contains:

- Supplementary material detailing the intermediate case of single defects and linear function, with additional figures
- Supplementary figure showing comparison with Stochastic Simulations

S1 Illustration of EGGTART on Examples of Intermediate Complexity

Two popular and well-studied special cases of the general inhomogeneous ℓ-TASEP are lattices with defect clusters and linear jumping rates. Here we detail how EGGTART recovers previously known results in these two examples, while allowing exploration of closely related models that so far had proven inaccessible.

Bottleneck induced by defect sites

Due to its relevance in applications and mathematical tractability, many studies of the TASEP have considered inhomogeneity created by defects, i.e., sites with slower rates **???**. For example, defects can be associated with "slow" codons that potentially limit the protein synthesis rate during mRNA translation **??**, or with structural imperfections of the microtubular structure or motor proteins transported along microtubules **??**. We illustrate the simplest case of a single defect in the top three panels of Figure **??**, before demonstrating the behavior of two disjoint defects in the bottom two panels. In the former case, mean-field approximations successfully approximate the phase diagram and density profiles **?????**. Compared with the homogeneous system, the main effects caused by a single defect are an enlarged MC phase region with a decrease of the maximal current, as well as significantly altered density profiles. LD and HD densities exhibit local deviations around the defect site, while in MC the defect site acts as a separator between a region of high density on the left and a region of low density on the right. For macroscopic clusters of defect sites, refined mean-field approaches have shown that these effects persist **??**. Using the hydrodynamic limit, we are able to recover these results precisely: Defining $\lambda(x) = 1 - \eta_\varepsilon(x)$, where η_ε is a suitably normalized bump function centered around the bottleneck x_0, we find that with $\lambda_{\min} = \lambda(x_0) < 1$,

$$\alpha^* = \beta^* = \frac{1}{1+\sqrt{\ell}}\left(1 - \sqrt{1-\lambda_{\min}}\right),$$
$$J_{\max} = \frac{\lambda_{\min}}{(1+\sqrt{\ell})^2},$$

leading to the reduction in transport capacity, shifts in the phase diagram and local density perturbations (top two panels in Figure **??**) outlined in the main manuscript. The coexistence of low and high density regions in the MC phase is reflected in the branch switching phenomenon (middle panel of Figure **??**). In addition, EGGTART allows to interactively explore the dynamics associated with the emergence of a second defect located downstream the first one (with respective rates $\lambda^{(2)}$ and $\lambda^{(1)}$). In the MC regime, an initial local distortion of ρ around the second bottleneck for $\lambda^{(1)} < \lambda^{(2)}$ turns into a global distortion as soon as $\lambda^{(2)} < \lambda^{(1)}$, as shown in the bottom two panels of Figure **??**.

Linear rate function

Monotonically-varying jump rates are another simple example of spatial inhomogeneity. This kind of pattern has been observed in translation dynamics, where the mean ribosome

elongation rate, obtained by averaging over all mRNA transcripts, increases between codon positions ~ 50 and 200, leading to the so-called "5' translational ramp" **?**. Such variation can be modeled to first approximation by a linear rate function $\lambda(x) = s(x-1)+1$ for $s \in [0,1]$ (the case of decreasing rates with $s < 0$ can be treated analogously). With $\lambda_{\min} = \lambda_0 = 1 - s$ and $\lambda_1 = 1$, we can easily compute α^* and β^* using the formulae obtained in **?**, obtaining for the particular case of $\ell = 1$,

$$\alpha^* = \frac{1-s}{2} \quad \text{and} \quad \beta^* = \frac{1}{2}\left(1 - \sqrt{s}\right),$$

reflecting the asymmetry of the model. Similarly, the phase boundary between LD and HD is explicitly given by the curve

$$\alpha(1 - \alpha - s) = \beta(1-\beta)(1-s),$$

recovering previous results obtained through mean-field approximations **?**. Notably, this curve is non-linear (see right half of Supplementary Figure **??**), again evidencing the asymmetry of the model. Since λ achieves its minimum at the lattice entry site, both LD and MC profiles are described by the lower branch (Supplementary Figure **??** top and bottom panel), allowing for densities larger than $\rho^* = (\ell + \sqrt{\ell})^{-1}$ only in HD (Supplementary Figure **??** middle panel). Lastly, we highlight a robustness property of this linear model, which so far has eluded attention: Lattices with linearly increasing jump rates belong to a family of systems (namely, those for which $\lambda_0 = \lambda_{\min}$) whose currents are *maximally insensitive* to fluctuations in the initiation rate α. This follows directly from our explicit description of the particle current J_L as a function of $\lambda_0, \lambda_{\min}$ and α, and is illustrated in Figure **??**. This description only became available through consideration of the full general inhomogeneous ℓ-TASEP, explaining why the role of λ_0 had remained unnoticed.

Robustness characterizations of particle currents like these, together with sensitivity constraints on particle densities, as illustrated in the bottom two panels of Figure **??**, have important consequences for optimizing ribosome usage and translation efficiency **?**. By allowing for immediate quantification of such phenomena, EGGTART enables users to assess the optimality of any given system and, if necessary, open avenues to improve its efficiency.

S2 Validation of EGGTART's accuracy

A detailed demonstration of the convergence speed associated with the hydrodynamic limit (and therefore, its accuracy when describing finite systems) has been carried out in **?**. As shown there, convergence is generally fast, with lattices as short as 100 sites typically producing particle currents and densities indiscernible from our hydrodynamic predictions. Figure **??** illustrates a simple instance of this validation study by comparing empirical samples of Monte-Carlo simulations for $\ell = 1$ and $N = 100$ to the theoretical profiles provided by EGGTART. For shorter lattice lengths, and longer lattice and particle lengths, as well as performance analyses based on phase state, we refer the reader to **?**. In particular, Figures 2, S3 and S6 of that reference demonstrate that hydrodynamic predictions indeed faithfully recover system statistics across a broad range of system configurations.

S3 Supplementary Figures

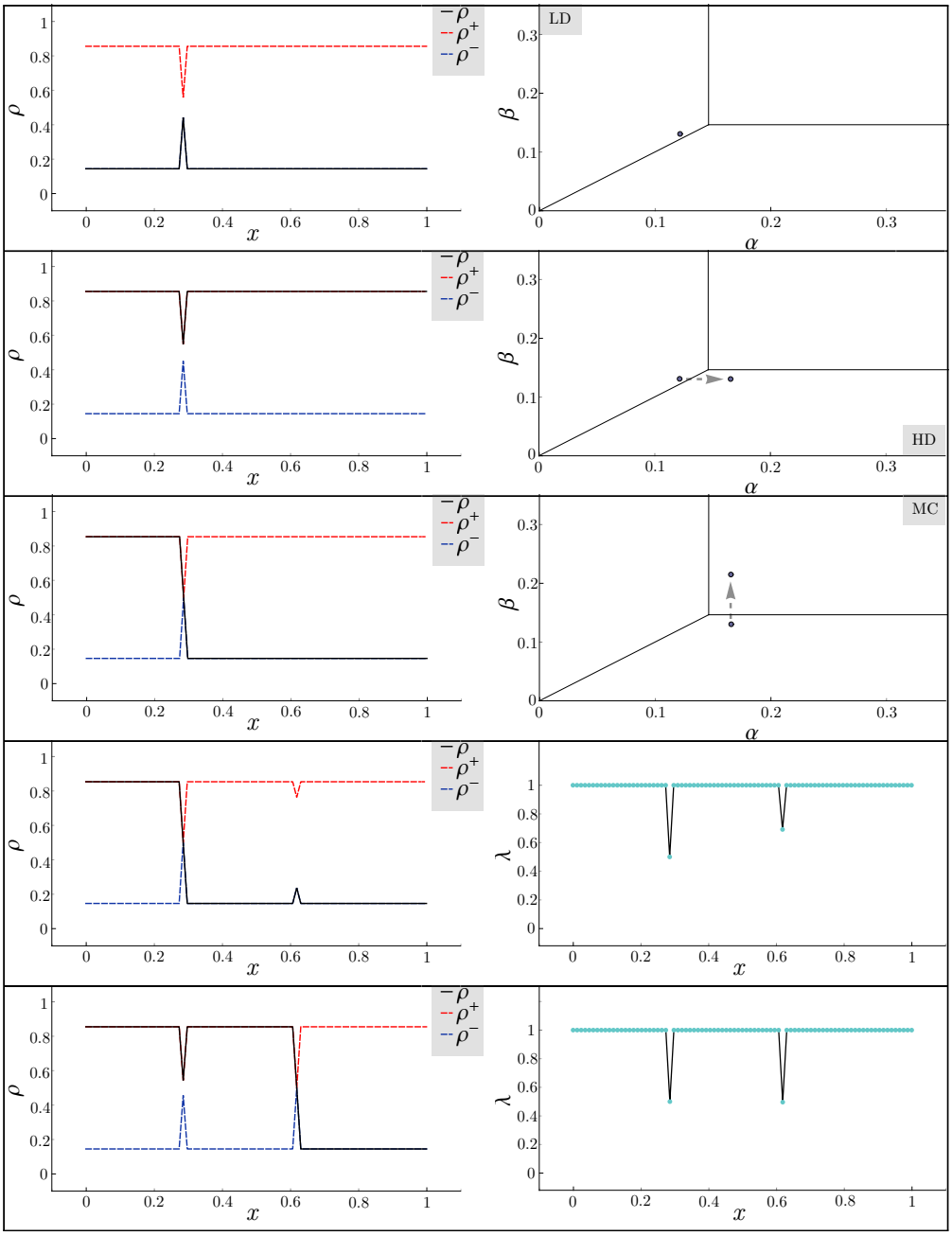

Figure S1. Interactive visualization on the example of defect clusters. EGGTART allows for convenient exploration of discontinuous phenomena around phase transitions (top three panels) and singular rate configurations (bottom two panels).

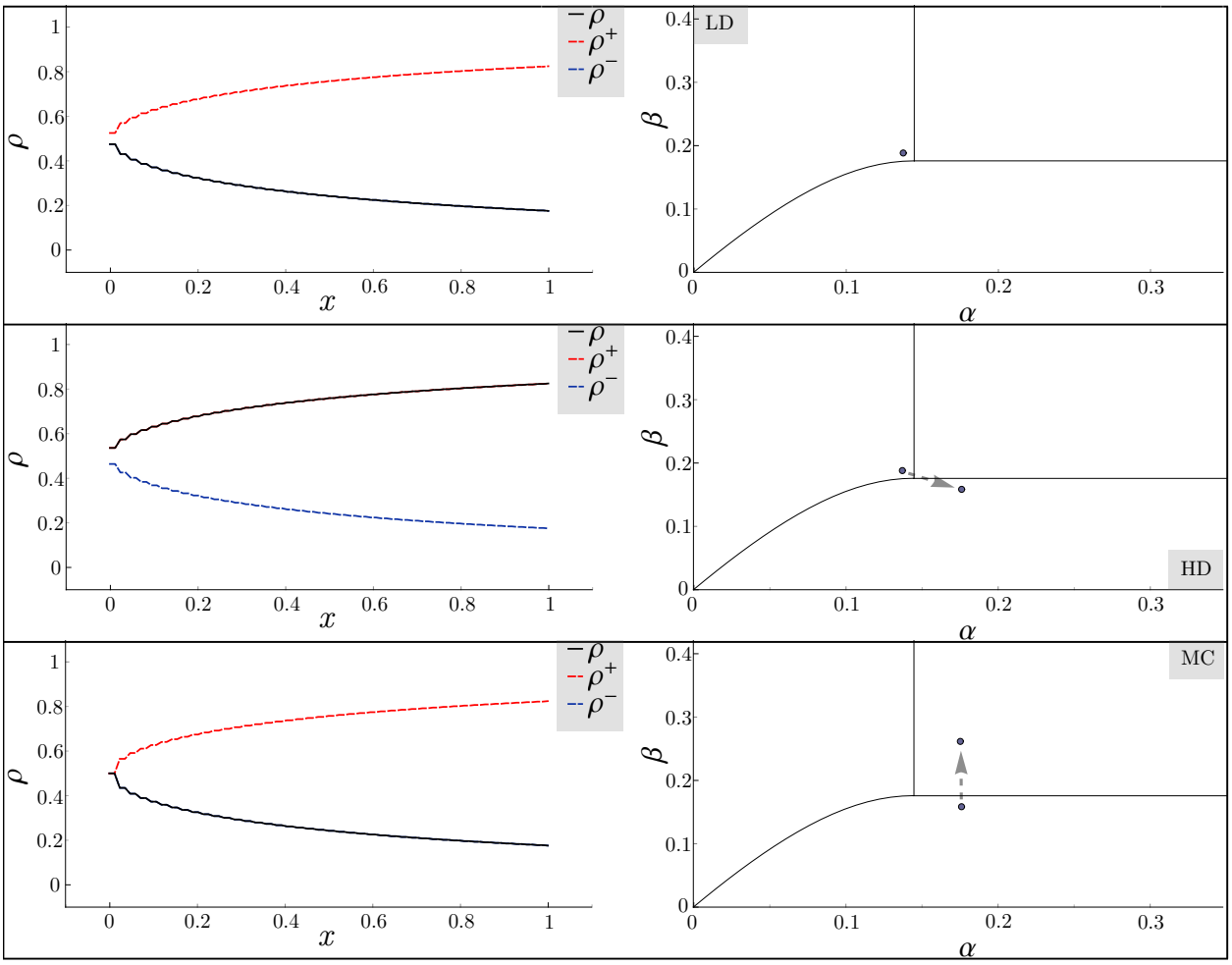

Figure S2. Interactive visualization on the example of linear rate functions. EGGTART correctly reproduces singular cases of the inhomogeneous ℓ-TASEP, when either $\lambda_0 = \lambda_{\min}$ (plotted here) or $\lambda_1 = \lambda_{\min}$, and LD and MC densities coincide.

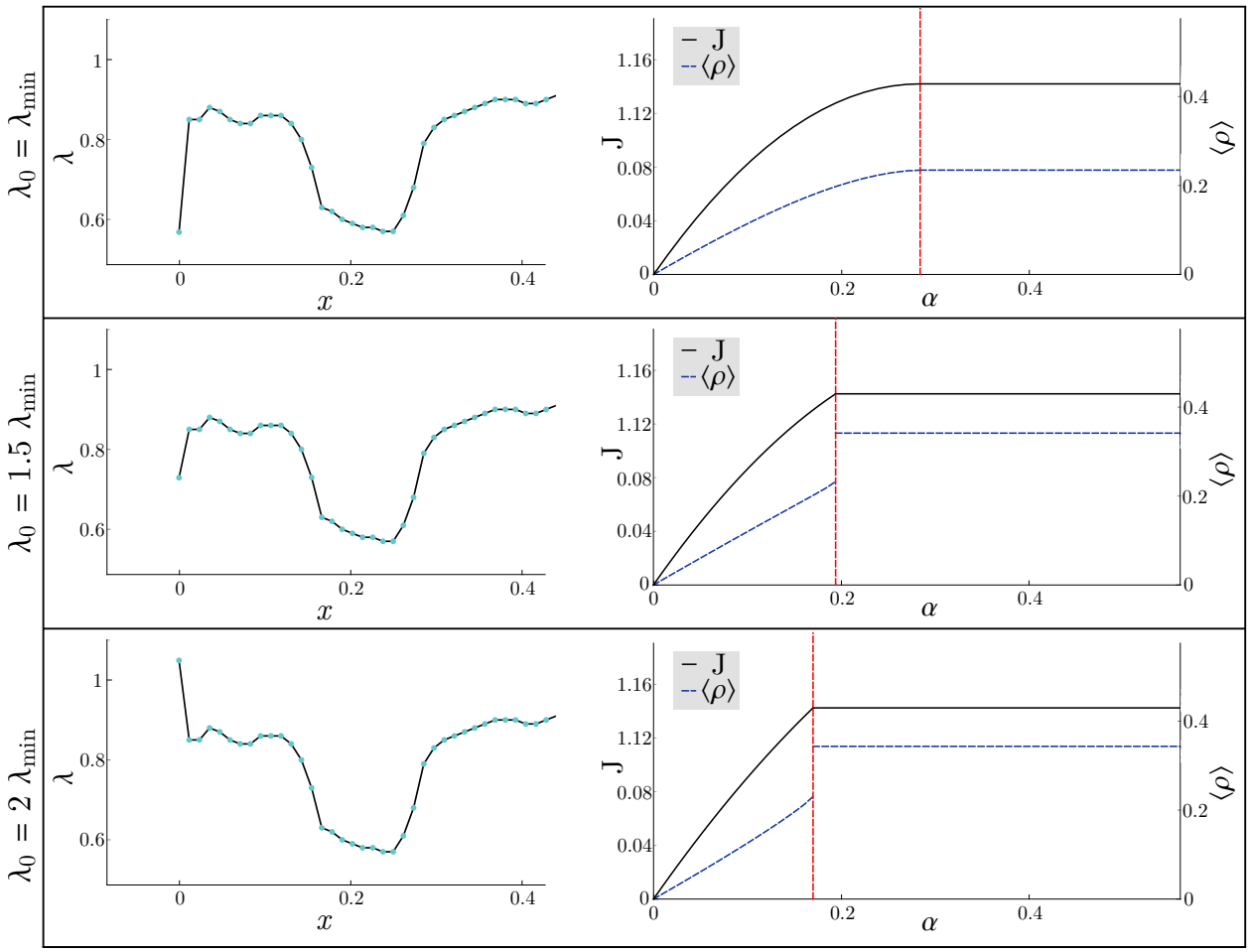

Figure S3. Impact of λ_0 on sensitivity. The precise effect of changes in the initial rate λ_0 on current J and mean density $\langle\rho\rangle_x = \int_0^1 \rho(x)\,\mathrm{d}x$ can be easily visualized using the interactive interface of EGGTART: Larger λ_0 lead to higher sensitivity of J to changes in α, and quicker saturation at maximum capacity. Moreover, $\langle\rho\rangle_x$ phase transitions are present only if $\lambda_0 > \lambda_{\min}$.

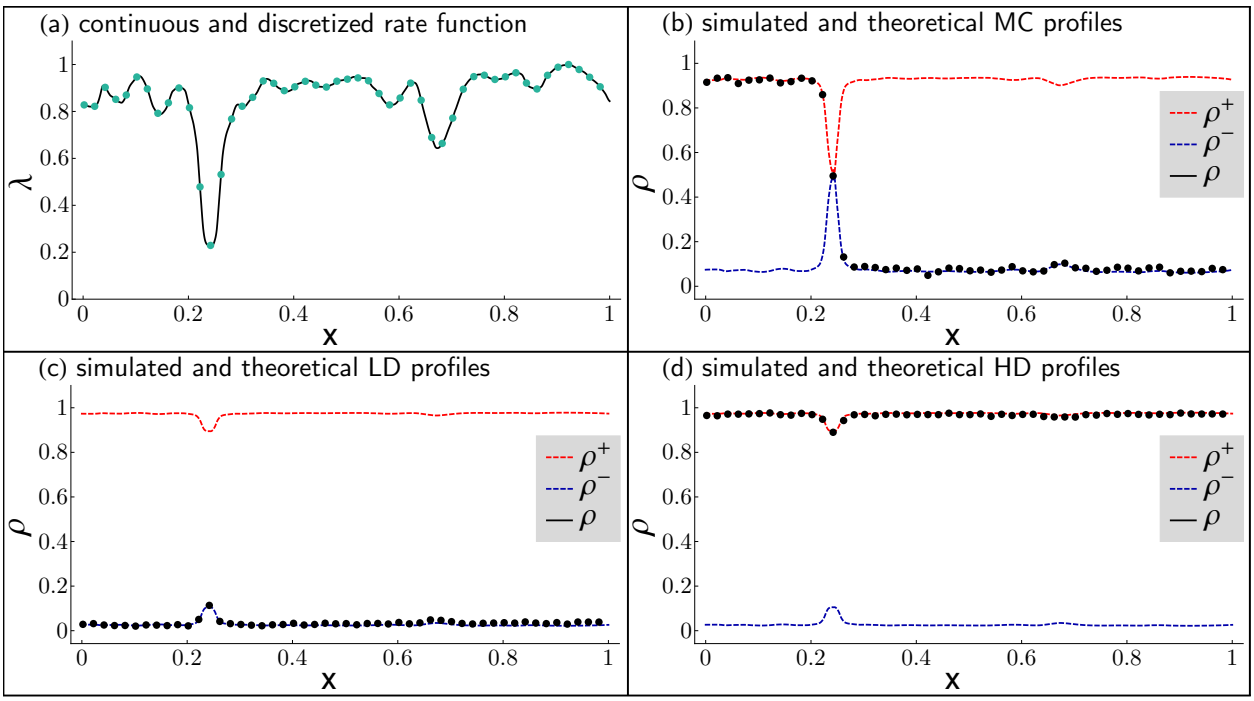

Figure S4. Comparison with Monte Carlo simulations. 5×10^7 Monte-Carlo iterations were averaged after 10^7 burn-in steps on a lattice of size 100, $\ell = 1$ particles and the rate function given in panel (a). The resulting simulated density profiles (in dots) agree well with our theoretical predictions in all regimes of the phase diagram, obtained by adjusting α and β.